analytical chemistry

pubs.acs.org/ac

Article

Mineralization of pH-Sensitive Doxorubicin Prodrug in ZIF-8 to Enable Targeted Delivery to Solid Tumors

Jiaqi Yan,[¶] Chang Liu,[¶] Qiwei Wu,[¶] Junnian Zhou, Xiaoyu Xu, Lirong Zhang, Dongqing Wang,* Fan Yang,* and Hongbo Zhang*

Cite This: *Anal. Chem.* 2020, 92, 11453−11461

Read Online

ACCESS | Metrics & More | Article Recommendations | Supporting Information

ABSTRACT: The zeolitic imidazolate framework (ZIF-8), composed of zinc ion and dimethylimidazole, is widely used in drug delivery because of the easy fabrication process and the good biosafety. However, ZIF-8 suffers from low affinity to nonelectric-rich drugs and does not have surface functional groups. Here, to deliver doxorubicin (DOX) with ZIF-8 to specific target sites, DOX was first modified with a pH-sensitive linker containing two carboxyl groups to form the inactive prodrug CAD and subsequently seeded inside ZIF-8 by a 5 min mineralization process. CAD has high affinity to ZIF-8 because of the carboxyl groups and can anchor to the ZIF-8 surface to enable the surface modification with folic acid for tumor targeting. Moreover, the DOX release is precisely controlled by three steps of acidic pH response, with the dissociation of the FA layer, the breakdown of the ZIF-8 structure, and the cleavage of the pH-sensitive linker in prodrug. This novel "prodrug-ZIF-8" strategy has opened a new horizon in drug delivery.

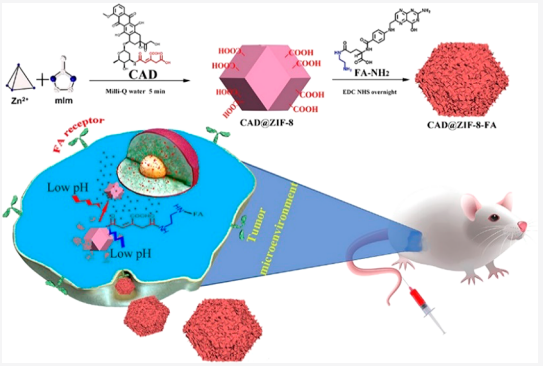

Nanomedicine enables specifical drug delivery at the target sites with controlled release, which shows great potential in cancer diagnosis and treatment.[1−3] Metal−organic frameworks (MOFs) composed of metal clusters and organic ligands, which have various advantages compared with many other available drug-delivery systems (DDSs) because of the defined crystal structure and the flexibility in the ascendant combination of both organic and inorganic.[4−7] Among different types of MOFs, the ZIF-8 system which is composed of Zn and dimethylimidazole is widely studied in the drug-delivery field because of the following: (1) The ZIF-8 system shows excellent biocompatibility at low concentration, since Zn is an essential element for the development of the human immune system and nervous system,[8] and imidazolyl is part of the amino acid histidine;[9] (2) ZIF-8 can be easily synthesized at room temperature in 5 min with tunable size, which can also be easily scaled up for future applications in the clinic;[10−13] (3) The ZIF-8 system has acidic-responsive degradation, which benefits its drug delivery to a tumor microenvironment and an intracellular environment.[14] Nevertheless, despite the many advantages of the ZIF-8 system, there are still some crucial issues that make it unable to fully meet the clinical needs for targeted drug delivery. For instance, (1) ZIF-8 NPs shows lower affinity with drugs that lack electric-rich groups like carboxyl groups, carbonyl, and so on. This character limits their loading capacity and causes undesired premature release of certain drugs;[15−17] (2) Since no active chemical groups exist on the ZIF-8 structure, the system bears poor surface functionalization ability for further active targeting design;[18,19] (3) It has been found that at high concentration, ZIF-8 NPs also show a toxic effect. Therefore, the doses must be limited.[14,20,21] Moreover, many other MOF candidates have suffered from similar drawbacks in biomedical applications.

To overcome these problems, different strategies have been investigated to improve the ZIF-8 system, such as surface coating by ZrO_2 or polydopamine to decrease the ZIF-8 toxicity[20] and carbonating ZIF-8 at 800 °C and then reacting it with $(NH_4)_2S_2O_8$ and concentrated H_2SO_4 to achieve surface carboxylation for postmodification.[22] However, these methods are complicated and need harsh reaction conditions; hence, they are difficult to scale up. Furthermore, the drug loading capacity cannot be improved with those methods.

Doxorubicin (DOX), a first-line anticancer drug, can inhibit cell proliferation by disturbing the synthesis of RNA and DNA. However, DOX lacks targeting ability and has strong cardiotoxicity; thus, more effective DOX delivery is still highly demanded. Prodrug strategies have been investigated in the design of DDSs. Modifying drugs into inactive prodrugs and releasing the parent drug after being triggered by specific

Received: June 17, 2020
Accepted: July 15, 2020
Published: July 15, 2020

https://dx.doi.org/10.1021/acs.analchem.0c02599
Anal. Chem. 2020, 92, 11453−11461

Scheme 1. Fabrication of CAD@ZIF-8-FA NPs as a Versatile Nanovehicle for i.v. Injection Cancer Treatment

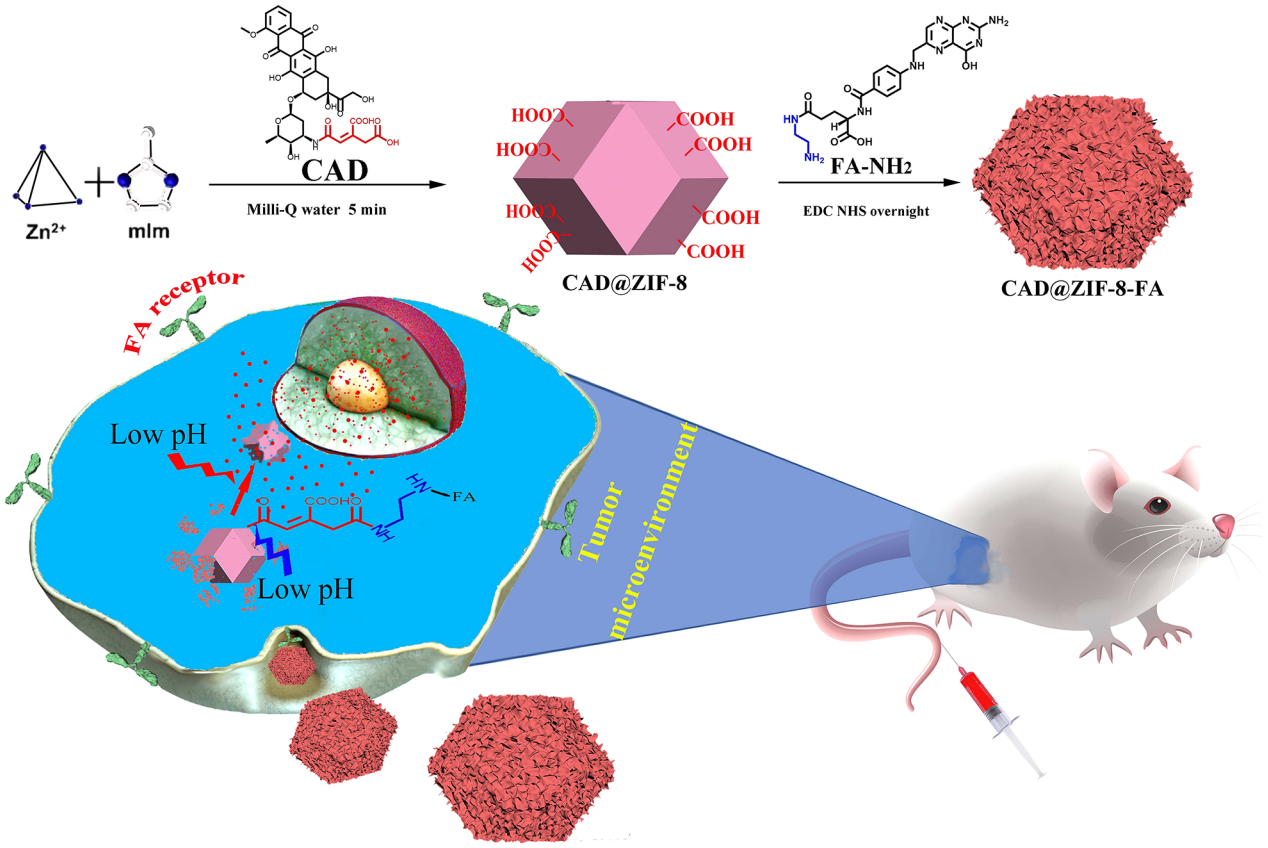

environments has been applied to reduce the drug toxicity and improve the target drug delivery.[23,24] It has been reported that after modifying paclitaxel (PTX) with 3,3′-dithiodipropionic acid, the toxicity of PTX apparently decreased and redox-mediate releasing ability was achieved.[25] Moreover, the modification can also introduce active reaction groups for further functionalization.

Herein, we have developed a proof of concept methodology for target-specific and pH-responsive delivery of DOX by ZIF-8 (Scheme 1). DOX was first modified by a pH-sensitive linker cis-aconitic anhydride (CAA), which contains two carboxyl groups and forms the prodrug CAD, and then the CAD was loaded into ZIF-8 NPs through a 5 min mineralization process. Since CAD has two carboxyl groups, the affinity to ZIF-8 can be significantly improved, thus achieve high loading degree and negligible burst release. Moreover, the carboxyl groups anchored to the ZIF-8 surface can be further conjugated with a tumor-targeting ligand to achieve targeted drug delivery. The pH-responsive nature of ZIF-8 and the CAD can further improve the tumor selectivity. Therefore, this simple and effective CAD@ZIF-8 platform has opened up a new horizon in drug delivery, which extends the MOF-based DDSs and the targeted delivery of DOX.

EXPERIMENTAL SECTION

Materials. Doxorubicin (DOX·HCl) and folic acid (FA) were purchased from Arisun ChemPharm Co., Ltd. (China). *cis*-Aconitic anhydride (CAA), ethylenediamine, 4-dimethylaminopyridine (DMAP), *N*-hydroxy succinimide (NHS), and *N*-(3-(dimethylamino)propyl)-*N*-ethylcarbodiimide hydrochloride (EDC·HCl) were purchased from Alfa Aesar (Finland). 2-Methylimidazole (MIM), Zn $(NO_3)2{\cdot}6H_2O$, *N*,*N*-dimethylformamide (DMF), triethylamine (TEA), dichloromethane (DCM), and menthol (MeOH) were purchased from Sigma-Aldrich (Finland).

Synthesis of CAD and FA-NH_2. Doxorubicin hydrochloride (200 mg) was dissolved in distilled water (20 mL) and cooled on ice. *cis*-Aconitic anhydride (300 mg) was dissolved in 1,4-dioxane (1 mL) and slowly added to the doxorubicin solution with continuous stirring. The pH of the reaction mixture was immediately adjusted to 9.0 and controlled in the range of 8.5−9.0 by carefully adding NaOH (0.5 M). The reaction mixture was placed in an ice bath for 20 min. Then the pH was adjusted to 7.0 with cold HCl (1 M), and the mixture was stirred for another 20 min. HCl (1 M) was added slowly to the mixture until a heavy precipitate (*cis*-aconitic anhydride-doxorubicin, CAD) was formed. Then the product was extracted with ethyl acetate (25 mL × 4) and evaporated. Folic acid was animated with ethylene diamine through the formation of an amide bridge. For the conjugation, folic acid (220 mg) has to be treated with ethylenediamine (3.2 mL), stirred overnight using EDC/NHS as catalyst, and then extracted in ether.

Synthesis of CAD@ZIF-8 and CAD@ZIF-8-FA. The prescription for different CAD loading ratios of CAD@ZIF-8 was tried and tested. Briefly, 135 mg of zinc nitrate and different amounts of CAD (0, 4, 8, 16, 32 mg) were dissolved in 2 mL of water, respectively, and sonicated for use. Next, 3.7 g of dimethylimidazole was dissolved in 8 mL of water, sonicated at 40 °C, and then poured into a 20 mL beaker with a 1 cm stir bar at 100 rpm. After that, the zinc nitrate and the CAD mixture were poured into the beaker instantly, stirred

https://dx.doi.org/10.1021/acs.analchem.0c02599
Anal. Chem. 2020, 92, 11453−11461

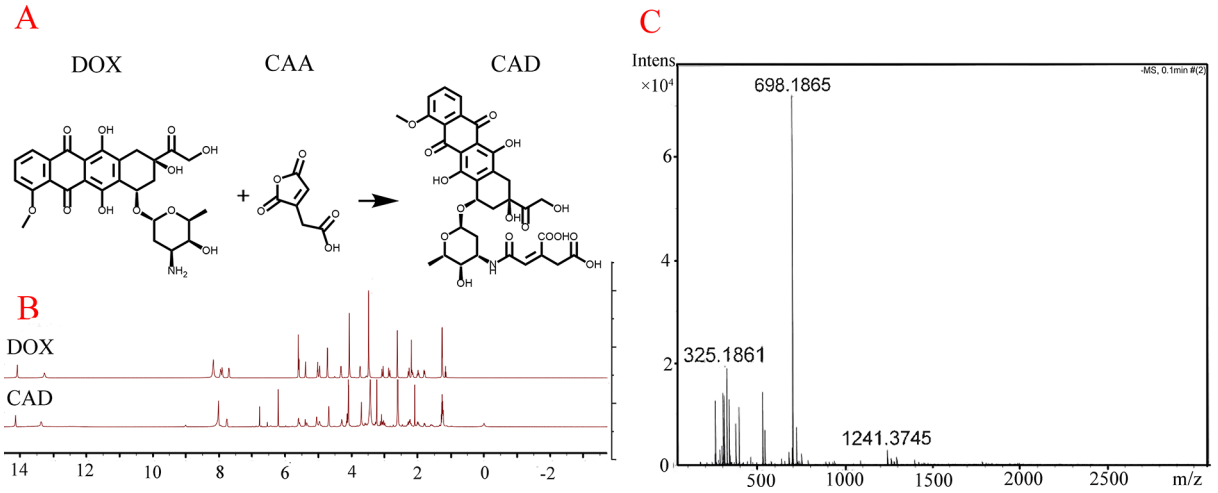

Figure 1. Nuclear magnetic spectrum and mass spectrometry results of prodrug CAD. (A) Synthesis route of CAD. (B) ^{1}H NMR spectra of CAD and DOX in DMSO-d_6. (C) MS spectra of CAD.

for 5 min, centrifuged at 16 000 rpm, and washed 3 times using milli-Q water; as a result, CAD@ZIF-8 was obtained. Subsequently, 20 mg of the different loading ratios of CAD @ ZIF-8 NPs was redispersed in 10 mL of water, separately, and 1.5 mg of EDC and 1.3 mg of NHS were added in each group. After activating the carboxyl groups of CAD which are on the surface of the nanoparticles for 1 h, 5 mg of FA-NH_2 was added for each loading ratio group. After being stirred overnight, centrifuged at 16 000 rpm, and washed 3 times, different loading ratios of CAD@ZIF-8-FA can be achieved.

Characterization of the CAD, FA-NH_2, and Nanoparticles. The ^{1}H NMR spectra of CAD, FA-NH_2 were recorded on Bruker 500 NMR spectrometers (Bruker, Billerica, MA, U.S.A.). Mass spectra were recorded for CAD on a Bruker Daltonics microTOF-Q mass spectrometer (Bruker, Billerica, MA, U.S.A.). In addition, the FTIR spectra of CAD, CAD@ZIF-8, and CAD@ZIF-8-FA were recorded on a Thermo Scientific Nicolet iS50 Fourier transform infrared spectrometer in the wavenumber of 400−4000 cm^{-1}. Particle sizing was performed using dynamic light scattering with Zetasizer Nano ZS (Malvern Instruments Ltd., U.K.). For each measurement, the sample (1.0 mL) was put in a disposable polystyrene cuvette (SARSTEDT AG & Co., Germany). The nanocarrier surface ζ-potential was measured with Zetasizer Nano ZS by using disposable folded capillary cells (DTS1070, Malvern, U.K.). Both the size and ζ-potential were recorded as the average of three measurements. The structure of the blank ZIF-8, CAD@ZIF-8, and CAD@ZIF-8-FA were evaluated by transmission electron microscope (TEM; JEOL 1400 Plus, JEOL, U.S.A.) at an acceleration voltage of 80 kV. The TEM samples were prepared by using a tweezer to hold the carbon-coated copper grids (200 mesh; Ted Pella, Inc., U.S.A.) and soaking them within the particle solution; they were then removed and dried in the air prior to imaging.

Characterization of Drug Loading Degree and Efficiency. The CAD loading degree (LC) and FA loading efficiency (LE) were calculated according to the following formulas (1) and (2):

$$\text{LC}\ (\%) = \frac{\text{entrapped drug}}{\text{weight of nanoparticles}} \times 100\% \quad (1)$$

$$\text{LE}\ (\%) = \frac{\text{total input of drug} - \text{amount of drug in the supernatant}}{\text{total input of drug}} \times 100\% \quad (2)$$

The DOX loading contents were quantified by gradient analytical HPLC assay. An HPLC assay was performed on an Agilent 1100 instrument, and 20 μL of solution was loaded onto a Waters reverse phase column (250 × 4.6 mm). Acetonitrile (TFA 0.1%):water (TFA 0.1%) (Acetonitrile increase from 5 to 95% with 20 min) was eluted at a flow rate of 1 mL/min at 490 nm by a UV detector (UV-975, Jasco). FA was detected by UV−vis absorption at 282 nm.

In Vitro Release of DOX. CAD@ZIF-8-FA was dispersed in 1.0 mL of PBS buffer solution (pH = 6; pH = 7.4) and then gently shaken at 37 °C in the darkroom. At selected time intervals, the solution was centrifuged at 16 000 rpm, and then 0.9 mL of supernatant was withdrawn and analyzed by HPLC. Subsequently, 0.9 mL of fresh medium was returned to the original solution and sonicated until the nanoparticles were dispersed well; the medium was then put back into the shaker. The standard curve detected by HPLC for DOX is $Y = 4.6348X - 0.0283$ (R = 0.9998). Here Y is UV absorption integral of DOX at 490 nm wavelengths; X is the concentration of DOX (μg).

In Vitro Assays. The drug efficacy in cancerous and healthy cells was determined by a WST-1 cell viability assay. MDA-MB-231 cancer cells and MCF-10A cells were incubated overnight in a 96-well-plate (3000 cells per well) in cell growth media at 37 °C with 5% CO_2. The following day, the cell growth media were replaced with fresh media containing a different concentration of CAD, DOX, CAD@ZIF-8, and CAD@ZIF-8-FA and incubated for 24 h. Free drug stock solutions (DOX, CAD) were prepared in DMSO, and nanoparticles were suspended in water. All the dilutions for the cell viability assay were prepared in cell growth media. After being incubated with free drug or nanoparticles, 10 μL of WST-1 reagent was added to each well, and the cells were incubated for 2 h at 37 °C with 5% CO_2. After incubation, the absorbance was measured by a Varioskan Flash Multimode Reader (Thermo Scientific Inc., Waltham, MA, U.S.A.) at 440 nm. The blank ZIF-8 concentration corresponds to the

https://dx.doi.org/10.1021/acs.analchem.0c02599
Anal. Chem. 2020, 92, 11453−11461

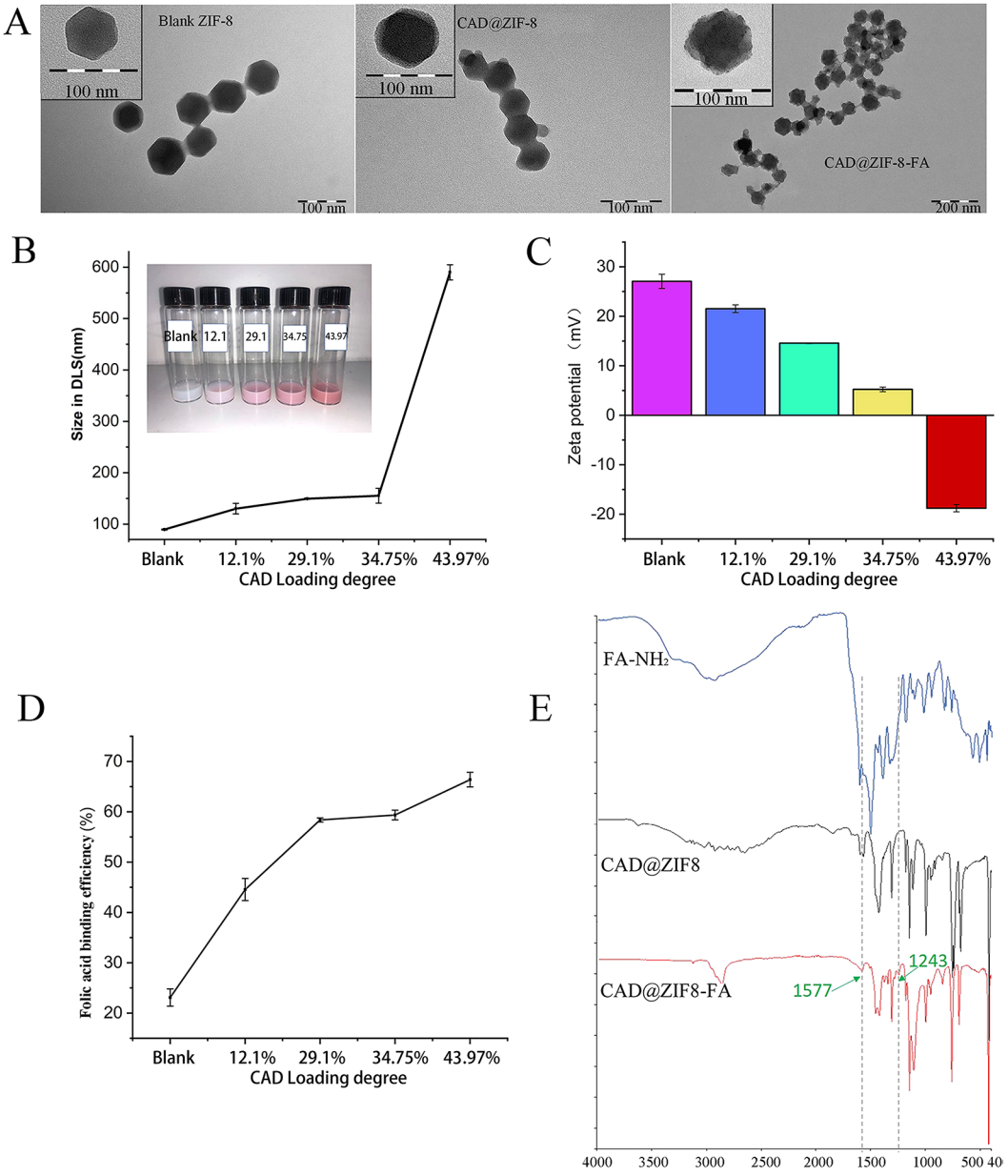

Figure 2. Characterization of blank ZIF-8, CAD@ZIF-8, and CAD@ZIF-8-FA NPs. (A) TEM images. (B) Size results from DLS. (C) Zeta potential of CAD@ZIF-8 with different concentrations of CAD. (D) Folic acid binding efficiency and (E) FTIR spectra (n = 3).

content of the ZIF-8 in each NPs at different loading ratio. For cell culture and maintenance, CLSM imaging, and flow cytometry assay, all the details are provided in the Supporting Information.

In Vivo Assays. All animal studies were performed in accordance with the Ethics Committee of Affiliated Hospital of Jiangsu University. huPBMC-NCG mice were established by implanting human peripheral blood mononuclear cells (PBMCs) into NCG mice. Human peripheral blood mononuclear cells (hPBMCs) were injected the caudal vein (1×10^7 cells) of NCG mice for huPBMC reconstitution. Subcutaneous inoculation of MDA-MB-231 cancer cells into the male NCG mice which were purchased from GemPharmatech. When the average body weight reached 19 g, the mice were randomly divided into four groups (six mice per group): the group treated with saline (200 μL) served as the control, while the other three groups were, respectively, injected with DOX, blank ZIF-8, and CAD@ZIF-8-FA (equal to 3 mg of DOX per gram mice, 200 μL), respectively, every 3 days for 19 days. Meanwhile, the mice were weighed, and the tumor volumes were measured every 3 days. The tumor volumes were calculated using the following equations: $V = (\text{length} \times \text{width}^2)/2$. The mice were euthanized at the end of the treatments for histological analysis. The tumors and major organs (including heart, liver, spleen, kidney, and lung) were harvested for routine staining with hematoxylin−eosin (H&E). The final images were obtained and analyzed under a microscope (IVIS Lumina XRMS Series III, Perkin Elmer).

RESULTS AND DISCUSSION

Synthesis and Characterization of CAD. DOX were fabricated into a prodrug CAD through a one-step ring-opening reaction.[26] The active carboxyl group within CAD not only can achieve high carrier affinity but also can realize

https://dx.doi.org/10.1021/acs.analchem.0c02599
Anal. Chem. 2020, 92, 11453−11461

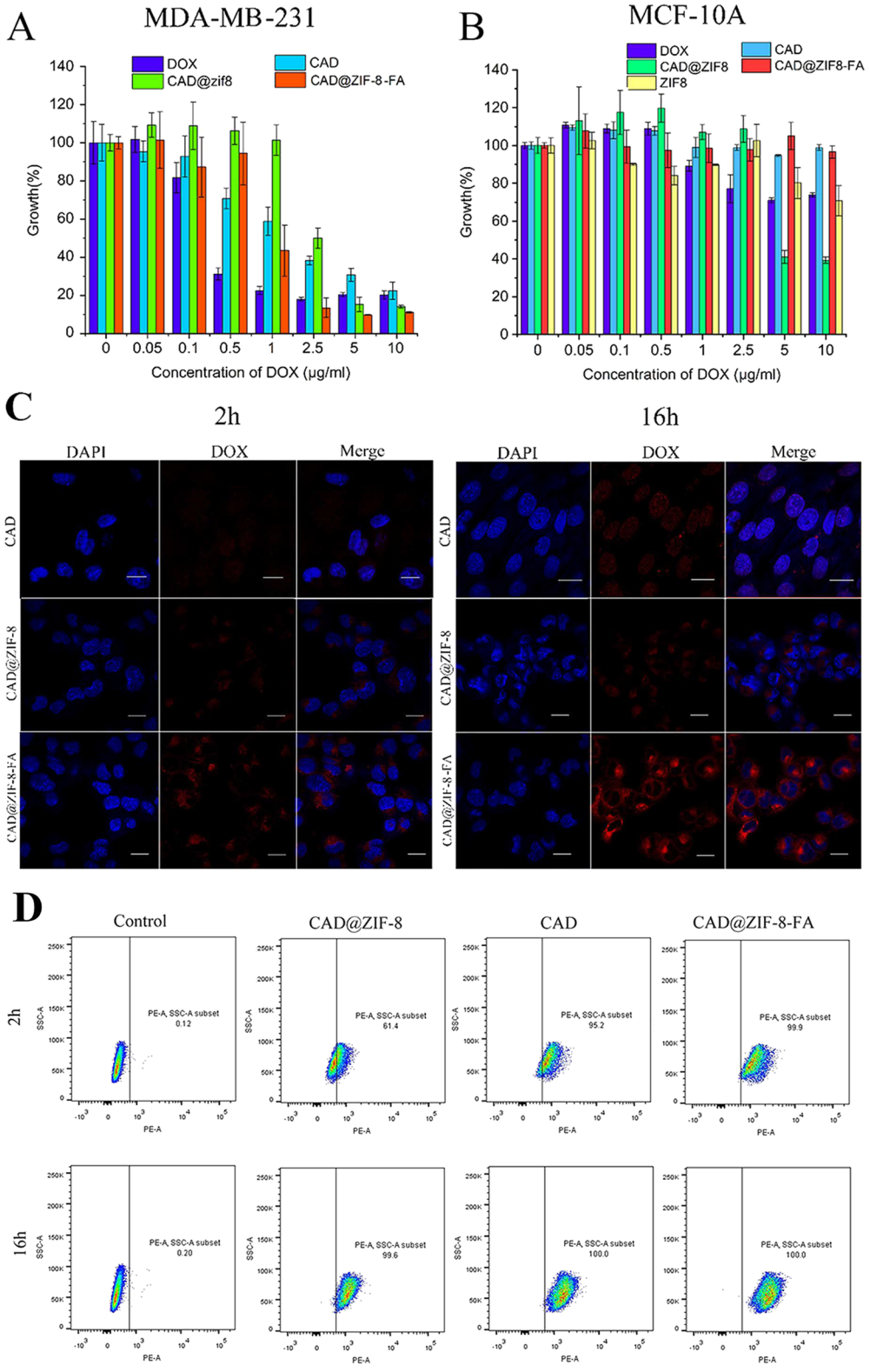

Figure 3. Cytotoxicity and cell uptake. (A) Cytotoxicity of DOX, CAD, CAD@ZIF-8, and CAD@ZIF-8-FA NPs for MDA-MB-231. (B) DOX, CAD, CAD@ZIF-8, CAD@ZIF-8-FA NPs, and blank ZIF-8 for MCF-10A. (C) Confocal microscopy images of CAD, CAD@ZIF-8, and CAD@ZIF-8-FA NPs uptake in cancer cells MDA-MB-231 at 2 and 16 h. The scale bars denote 20 μm. (D) Flow cytometry of cellular uptake of the control group, CAD, CAD@ZIF-8, and CAD@ZIF-8-FA at 2 and 16 h, respectively, for MDA-MB-231.

carboxylation of ZIF-8 for further folate conjugation. The synthetic scheme was shown in Figure 1A. The ^{1}H NMR spectra shows that after modifying DOX by *cis*-aconitic anhydride (CAA), new peaks at 6.1 and 6.8 ppm were found, which were attributed to the protons (CH−COO−) of the CAA within the structure of CAD (Figure 1B). Moreover, the MS spectra of CAD (Figure 1C) gave a peak at a mass of 698.1865, corresponding to the calculated mass of 698.1727.

https://dx.doi.org/10.1021/acs.analchem.0c02599
Anal. Chem. 2020, 92, 11453−11461

Furthermore, the successful preparation of CAD prodrug was also confirmed by HPLC. We can see that the DOX and CAD had different peaks with retention times of 4.957 and 12.428 min, respectively (Figure S1). Therefore, MS, NMR, and HPLC results together confirmed that the CAD was successfully synthesized.

Synthesis and Characterization of CAD@ZIF-8 and CAD@ZIF-8-FA NPs. CAD@ZIF-8 particles were synthesized in pure aqueous solutions for 5 min at room temperature.[27] The transmission electron microscopy (TEM) images (Figure 2A and Figure S2) revealed that when increasing the loading degree from 12.1% to 43.97%, the size of NPs changed from 80 to 450 nm. Meanwhile, the hydrodynamic size measured by dynamic light scattering (DLS) (Figure 2B) were 159 to 590 nm, which consisted well with the TEM image. More importantly, the CAD attached layer and ZIF-8 corners were found and marked with arrows at 43.97% CAD loading degree (Figure S2), indicating that with the increased CAD loading degree, CAD formed an attachment layer on the ZIF-8 surface.

As shown in Figure 2C, we found that when loading degree was enhanced from 0 to 34.75%, the zeta potential only decreased 16.3 mV, whereas when the loading degree was increased from 34.75% to 43.97%, a 23.9 mV decrease was found. These results suggested that CAD was mineralized by ZIF-8 and the zeta potential was significantly affected at higher CAD loading degree.

On the basis of the characterization results of CAD@ZIF-8, we chose CAD@ZIF-8 NPs with 34.75% of CAD loading for later FA conjugating. To enable the conjugation, we modified the FA with ethylenediamine for a later amidation reaction. The NMR results of FA-NH_2 are shown in Figure S3. After incubation, a significant FA layer was observed in the CAD@ZIF-8-FA NPs (Figure 2A) even after extensive washing and sonication, and the zeta potential decreased to -10 ± 1.03 mV (Figure S4). Meantime, Figure 2D indicated that the blank ZIF-8 had low FA binding efficiency of 25%. However, when CAD loading degree was increased from 12.1% to 43.97%, the FA loading efficiency increased from 44% to 67.4%. As mentioned above, when CAD loading degree increases, more CAD will be coordinated on the ZIF-8 surface and facilitate the FA conjugation, therefore enhancing the FA binding efficiency. Moreover, the FTIR results (Figure 2E) showed two new peaks at 1577 and 1243, which were attributed to the newly formed amide bond.[28] Those results proved that the FA is covalently binding instead of physical absorbing to the CAD@ZIF-8.

In Vitro Release of DOX. Taking advantage of the FA surface modification, pH-sensitivity of ZIF-8, and prodrug, the release of DOX within an acid tumor environment requires three steps, which greatly enhances the releasing selectivity (Figure S5). The first step is the cleavage of the pH-sensitive linker between "CAD-FA" on the surface of ZIF-8, which in turn exposes the ZIF-8 NPs. The second step is the pH-sensitive degradation of ZIF-8 NPs and then release of the prodrug CAD. The third step is the pH-sensitive breakage of the linker in the prodrug and then release of the parent drug DOX.

Cytotoxicity Assays. To further evaluate the cytotoxicity of CAD@ZIF-8-FA NPs, a standard in vitro WST-1 assay was performed. From the results of Figure 3A, CAD@ZIF-8-FA NPs exhibited a strong tumor-killing ability for MDA-MB-231 cells. Meanwhile, we also found that pure DOX exhibits more toxicity when DOX concentration was lower than 1 $\mu g\ mL^{-1}$, while CAD@ZIF-8-FA NPs showed more toxicity at high concentration ($\geq 2.5\ \mu g\ mL^{-1}$). This may have occurred because the prodrug had less toxicity than parent drug under the same cultivated time, while at high concentration, the ZIF-8 carriers have enhanced the toxicity of DOX.

Meanwhile, the results of the healthy cell MCF-10A showed that the CAD and CAD@ZIF-8-FA groups had no toxicity for healthy cells even at a high concentration of 10 $\mu g\ mL^{-1}$ (Figure 3B). However, at a DOX concentration of 10 $\mu g\ mL^{-1}$, the cell variability was approximately 70%, and similar results were found with the pure ZIF-8. In the CAD@ZIF-8 group, the cell variability was around 40%. These results indicated that at high concentration, ZIF-8 and CAD@ZIF-8 NPs can induce cell toxicity for both healthy cells and tumor cells, while the FA layer can protect against toxicity in healthy cells and induce tumor-selective killing.

To investigate whether zinc will enhanced the toxicity of DOX, we performed the WST-1 assay with Zn^{2+} ion, ZIF-8, DOX, DOX + Zn^{2+}, and DOX + ZIF-8 groups (Figure S6). The results showed that zinc ions (corresponding with the DOX concentration in NPs) did not increase the toxicity of DOX, but a positive charge of CAD@ZIF-8 NPs may cause the enhanced cell uptake and then enhance the toxicity.

CLSM Imaging and Flow Cytometry Assay. Subsequently, to more intuitively observe the drug phagocytosis inside the cell, we conducted confocal experiments. The fluorescence excitative wavelength of CAD is similar to DOX as reported previously.[29] However, its fluorescent behavior in the presence of cells is unknown. Hence, as shown in Figure S7, we detected and found that the PE channel for DOX detection is also good for detecting CAD.

From CAD groups in Figure 3C, a small amount of red signal was found in cells within 2 h. This may occurred because the prodrug CAD was converted into the parent drug DOX in the acidic tumor microenvironment, then enter the nuclei to achieve the therapeutic effect (Figure S7). For the NPs groups, the CLSM and flow cytometry indicated that the CAD@ZIF-8-FA NPs showed significantly higher uptake than CAD@ZIF-8 (Figure 3C,D) in the MDA-MB-231 cancer cells, which was induced by folic-mediated endocytosis. Whereas, CAD@ZIF-8 and CAD@ZIF-8-FA particles were presented only in the cytoplasm after 2 h and accumulated around the cell nuclei (Figure 3C). These phenomenon illustrated that NPs had controlled the DOX release in the beginning.

Then we also investigated the localization of the drug in MCF-10A healthy cells using CLSM. As shown in Figure S8, for the CAD group of MCF-10A cells, since there is a lack of acidic environment, negatively charged CAD cannot break to form DOX, and only weak red fluorescence was found inside the nuclei within 16 h. Meanwhile, the CAD@ZIF-8-FA NPs showed almost no red signal in MCF-10A, whereas CAD@ZIF-8 NPs showed clear red signal in the cells (Figure S8). This was in good agreement with the WST-1 results in Figure 3B; these results indicate that FA modification has converted the positively charged particles to negatively charged particles, thus preventing the unspecific uptake to healthy cells and reducing the toxicity of the ZIF-8 carrier at high concentration.

In Vivo Assays. We next investigated the tumor suppression of the NPs by intravenous tail injection of PBS, blank ZIF-8, pure DOX, and CAD@ZIF-8-FA NPs into

https://dx.doi.org/10.1021/acs.analchem.0c02599
Anal. Chem. 2020, 92, 11453−11461

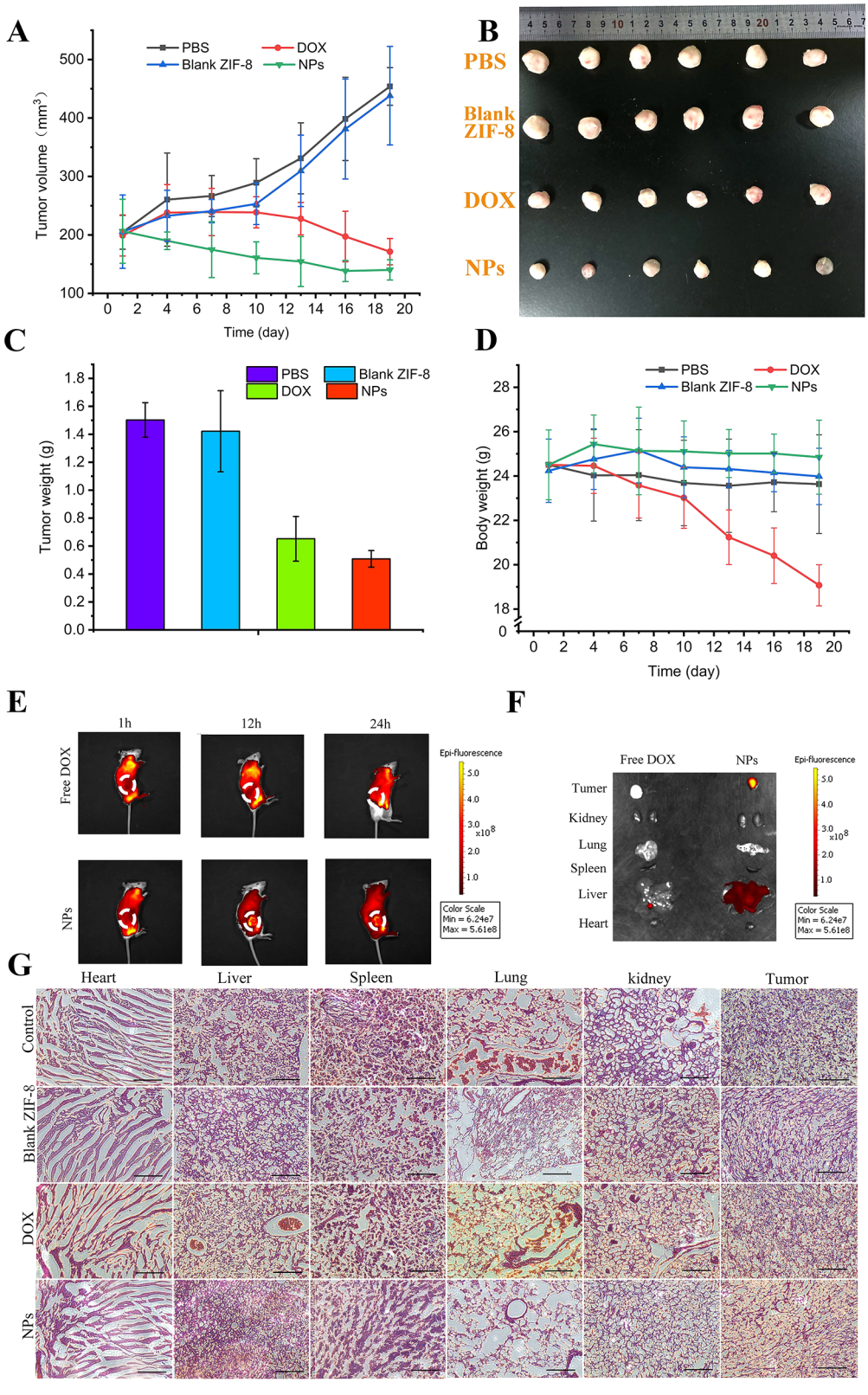

Figure 4. In vivo antitumor therapy. (A) Change of tumor volume during treatment. (B) Photo of tumors from different groups. (C) Tumor weight change during therapy. (D) Bodyweight changes during the treatment. (E) In vivo fluorescence imaging of MDA-MB-231 bearing mice at 1, 12, 24, 48, and 72 h after the injection of free DOX and CAD@ZIF-8-FA NPs. (F) Ex vivo bioluminescence imaging of different organs. (G) H&E staining of different organs.

different groups of tumor-bearing mice. The tumor growth curves in Figure 4A showed that the tumor volume was significantly reduced in the CAD@ZIF-8-FA NPs-treated mice, and the therapeutic effect was stronger than pure DOX. After the mice were sacrificed, from the photos of excised organs (Figure 4B) and the tumor weight (Figure 4C) of each

https://dx.doi.org/10.1021/acs.analchem.0c02599
Anal. Chem. 2020, 92, 11453−11461

group, we can visually observe that the CAD@ZIF-8-FA NPs group had the best treatment effect. Also, we observed that the weight of the mice was markedly reduced in the DOX-treated group but slightly increased in the CAD@ZIF-8-FA NPs-treated group, indicating that NPs can effectively reduce the side effects of DOX (Figure 4D).

To observe the distribution of CAD@ZIF-8-FA NPs in mice, we performed in vivo fluorescence imaging at 1, 12, and 24 h. We found that the NPs obviously accumulated at the tumor sites at 12 and 24 h, while DOX spread to the whole body of the mice (Figure 4E). The near infrared fluorescence imaging results of each organ in the DOX group and NPs group (Figure 4F) showed that the NPs group had the strongest red fluorescence in tumors. These results indicated that CAD@ZIF-8-FA NPs can promote the accumulation of drugs in tumors and increase the drug-delivery efficiency.

Afterward, we also performed a histological evaluation for saline, free DOX, blank ZIF-8, and CAD@ZIF-8-FA NPs groups. Because of the cytotoxic effect of CAD@ZIF-8-FA NPs on tumor cells, less nuclear staining was found in tumors because the cell nucleus will shrink and even lysis (Figure 4G and Figure S9). Furthermore, for the DOX-treated mice, the heart cells exhibit abnormal morphology because of the strong cardiotoxicity of DOX (Figure 4G and Figure S9), while no cardiotoxicity was found in the NPs group. Thus, these results indicated that the CAD@ZIF-8-FA nanoplatform was a promising DDS for targeted cancer therapy with low system toxicity.

CONCLUSIONS

In conclusion, we combined the merits of the ZIF-8 system and the prodrug strategy, and we fabricated a novel "prodrug-ZIF-8" nanoplatform for targeted DOX delivery. With this design, we solved several drawbacks of both prodrug and ZIF-8 systems. ZIF-8 carried the prodrug CAD to accumulate at the tumor site with an EPR effect. The prodrug introduced new carboxyl groups, which greatly improved the drug loading efficiency and prevented the premature release. In addition, the surface-anchored CAD also enabled the FA conjugation to form a FA layer to reduce the healthy cell uptake and enable the folic acid receptor mediated uptake in tumor cells. Moreover, the system has three steps of pH responsiveness, and the DOX release was precisely controlled. The in vitro and in vivo results showed that the FA-modified NPs could achieve tumor-selective therapeutics, accumulate at tumor site, and significantly inhibited the tumor growth and greatly reduced the cardiotoxicity of DOX. Overall, this i.v. injectable folate-surface-functionalized ZIF-8-based nanoplatform is a promising delivery system for cancer therapy. More importantly, this prodrug strategy method opens a new horizon for the surface modification of other MOFs systems.

ASSOCIATED CONTENT

Supporting Information

The Supporting Information is available free of charge at https://pubs.acs.org/doi/10.1021/acs.analchem.0c02599.

Cell culture and maintenance; CLSM imaging; flow cytometry assay; Figure S1−S9 (PDF)

AUTHOR INFORMATION

Corresponding Authors

Dongqing Wang − *Department of Radiology, Affiliated Hospital of Jiangsu University, Jiangsu University, 212001 Zhenjiang, P.R. China*; Email: wangdongqing71@163.com

Fan Yang − *The Center for Drug Research and Development, Guangdong Pharmaceutical University, Guangzhou, Guangdong 510006, China*; Email: gzyangfan@hotmail.com

Hongbo Zhang − *Pharmaceutical Sciences Laboratory and Turku Bioscience Center, Åbo Akademi University, FI-20520 Turku, Finland*; orcid.org/0000-0002-1071-4416; Email: hongbo.zhang@abo.fi

Authors

Jiaqi Yan − *The Center for Drug Research and Development, Guangdong Pharmaceutical University, Guangzhou, Guangdong 510006, China; Pharmaceutical Sciences Laboratory and Turku Bioscience Center, Åbo Akademi University, FI-20520 Turku, Finland*

Chang Liu − *Pharmaceutical Sciences Laboratory and Turku Bioscience Center, Åbo Akademi University, FI-20520 Turku, Finland*

Qiwei Wu − *Department of Radiology, Affiliated Hospital of Jiangsu University, Jiangsu University, 212001 Zhenjiang, P.R. China*

Junnian Zhou − *Experimental Hematology and Biochemistry Lab, Beijing Institute of Radiation Medicine, Beijing 100850, China*

Xiaoyu Xu − *Pharmaceutical Sciences Laboratory and Turku Bioscience Center, Åbo Akademi University, FI-20520 Turku, Finland*

Lirong Zhang − *Department of Radiology, Affiliated Hospital of Jiangsu University, Jiangsu University, 212001 Zhenjiang, P.R. China*

Complete contact information is available at: https://pubs.acs.org/10.1021/acs.analchem.0c02599

Author Contributions

¶J.Y., C.L., and Q.W. contributed equally to this work.

Notes

The authors declare no competing financial interest.

ACKNOWLEDGMENTS

This work was supported by Distinguished Clinical Investigator Grant of Jiangsu Province, China (Grant No. JSTP201701), Jiangsu Provincial Key Research and Development Programme (Grant No. BE2018690), Academy of Finland (Grant No. 328933), and Sigrid Jusélius Foundation (decision no. 28002247K1). F.Y. acknowledges grants from the Technological Project of Guangzhou Technology Bureau (Grant No. 20170402199).

REFERENCES

(1) White, M. C.; Holman, D. M.; Goodman, R. A.; Richardson, L. C. *Gerontologist* **2019**, *59* (Supplement_1), S1−S6.

(2) Miller, K. D.; Nogueira, L.; Mariotto, A. B.; Rowland, J. H.; Yabroff, K. R.; Alfano, C. M.; Jemal, A.; Kramer, J. L.; Siegel, R. L. *Ca-Cancer J. Clin.* **2019**, *69* (5), 363−385.

(3) Bray, F.; Ferlay, J.; Soerjomataram, I.; Siegel, R. L.; Torre, L. A.; Jemal, A. *Ca-Cancer J. Clin.* **2018**, *68* (6), 394−424.

(4) Abanades Lazaro, I.; Abanades Lazaro, S.; Forgan, R. S. *Chem. Commun. (Cambridge, U. K.)* **2018**, *54* (22), 2792−2795.

(5) Wuttke, S.; Dietl, C.; Hinterholzinger, F. M.; Hintz, H.; Langhals, H.; Bein, T. *Chem. Commun. (Cambridge, U. K.)* **2014**, *50* (27), 3599−601.
(6) Qin, J.; Cho, M.; Lee, Y. *ACS Appl. Mater. Interfaces* **2019**, *11* (12), 11743−11748.
(7) Dodson, R. A.; Wong-Foy, A. G.; Matzger, A. J. *Chem. Mater.* **2018**, *30* (18), 6559−6565.
(8) Jia, B.; Yang, H.; Han, Y.; Zhang, Z.; Qu, X.; Zhuang, Y.; Wu, Q.; Zheng, Y.; Dai, K. *Acta Biomater.* **2020**, *108*, 358−372.
(9) Griffiths-Jones, S.; Grocock, R. J.; van Dongen, S.; Bateman, A.; Enright, A. J. *Nucleic Acids Res.* **2006**, *34*, D140.
(10) Sun, C. Y.; Qin, C.; Wang, X. L.; Yang, G. S.; Shao, K. Z.; Lan, Y. Q.; Su, Z. M.; Huang, P.; Wang, C. G.; Wang, E. B. *Dalton Trans* **2012**, *41* (23), 6906−6909.
(11) Shi, J.; Wang, X.; Zhang, S.; Tang, L.; Jiang, Z. *J. Mater. Chem. B* **2016**, *4* (15), 2654−2661.
(12) Pan, Y.; Liu, Y.; Zeng, G.; Zhao, L.; Lai, Z. *Chem. Commun. (Cambridge, U. K.)* **2011**, *47* (7), 2071−2073.
(13) Lan, X.; Huang, N.; Wang, J.; Wang, T. *Chem. Commun. (Cambridge, U. K.)* **2018**, *54* (6), 584−587.
(14) Zheng, H.; Zhang, Y.; Liu, L.; Wan, W.; Guo, P.; Nystrom, A. M.; Zou, X. *J. Am. Chem. Soc.* **2016**, *138* (3), 962−968.
(15) Zhang, F. M.; Dong, H.; Zhang, X.; Sun, X. J.; Liu, M.; Yang, D. D.; Liu, X.; Wei, J. Z. *ACS Appl. Mater. Interfaces* **2017**, *9* (32), 27332−27337.
(16) Zheng, C. C.; Wang, Y.; Phua, S. Z. F.; Lim, W. Q.; Zhao, Y. L. *ACS Biomater. Sci. Eng.* **2017**, *3* (10), 2223−2229.
(17) Tiwari, A.; Singh, A.; Garg, N.; Randhawa, J. K. *Sci. Rep.* **2017**, *7*, 12598.
(18) Zhang, H.; Jiang, W.; Liu, R.; Zhang, J.; Zhang, D.; Li, Z.; Luan, Y. *ACS Appl. Mater. Interfaces* **2017**, *9* (23), 19687−19697.
(19) Roder, R.; Preiss, T.; Hirschle, P.; Steinborn, B.; Zimpel, A.; Hohn, M.; Radler, J. O.; Bein, T.; Wagner, E.; Wuttke, S.; Lachelt, U. *J. Am. Chem. Soc.* **2017**, *139* (6), 2359−2368.
(20) Su, L.; Wu, Q.; Tan, L.; Huang, Z.; Fu, C.; Ren, X.; Xia, N.; Chen, Z.; Ma, X.; Lan, X.; Zhang, Q.; Meng, X. *ACS Appl. Mater. Interfaces* **2019**, *11* (11), 10520−10531.
(21) Wu, Q.; Niu, M.; Chen, X.; Tan, L.; Fu, C.; Ren, X.; Ren, J.; Li, L.; Xu, K.; Zhong, H.; Meng, X. *Biomaterials* **2018**, *162*, 132−143.
(22) Cao, X.; Xia, J.; Meng, X.; Xu, J.; Liu, Q.; Wang, Z. *Adv. Funct. Mater.* **2019**, *29* (34), 1902237.
(23) Walther, R.; Rautio, J.; Zelikin, A. N. *Adv. Drug Delivery Rev.* **2017**, *118*, 65−77.
(24) Bildstein, L.; Dubernet, C.; Couvreur, P. *Adv. Drug Delivery Rev.* **2011**, *63* (1−2), 3−23.
(25) Yan, J.; Xu, X.; Zhou, J.; Liu, C.; Zhang, L.; Wang, D.; Yang, F.; Zhang, H. *ACS Applied Bio Materials* **2020**, *3*, 1216−1225.
(26) Du, C.; Deng, D.; Shan, L.; Wan, S.; Cao, J.; Tian, J.; Achilefu, S.; Gu, Y. *Biomaterials* **2013**, *34* (12), 3087−3097.
(27) Benzaqui, M.; Semino, R.; Menguy, N.; Carn, F.; Kundu, T.; Guigner, J. M.; McKeown, N. B.; Msayib, K. J.; Carta, M.; Malpass-Evans, R.; Le Guillouzer, C.; Clet, G.; Ramsahye, N. A.; Serre, C.; Maurin, G.; Steunou, N. *ACS Appl. Mater. Interfaces* **2016**, *8* (40), 27311−27321.
(28) Mallamace, F.; Corsaro, C.; Mallamace, D.; Vasi, S.; Vasi, C.; Dugo, G. *Comput. Struct. Biotechnol. J.* **2015**, *13*, 33−7.
(29) Hu, G.; Zhang, H.; Zhang, L.; Ruan, S.; He, Q.; Gao, H. *Int. J. Pharm.* **2015**, *496* (2), 1057−68.

https://dx.doi.org/10.1021/acs.analchem.0c02599
Anal. Chem. 2020, 92, 11453−11461